

Astreaks: Astrometry of NEOs with trailed background stars

Kritti Sharma,^{1,2,*} Harsh Kumar,^{3,†} Harsh Choudhary,³ Varun Bhalerao,³ Vishwajeet Swain,³ Bryce Bolin,^{1,4} G.C. Anupama,⁵ Sudhanshu Barway,⁵ Simran Joharle,⁶ Vedant Shenoy³

¹ Division of Physics, Mathematics, and Astronomy, California Institute of Technology, Pasadena, CA 91125, USA

² Department of Mechanical Engineering, Indian Institute of Technology Bombay, Powai, 400 076, India

³ Physics Department, Indian Institute of Technology Bombay, Powai, 400 076, India

⁴ Goddard Space Flight Center, 8800 Greenbelt Road, Greenbelt, MD 20771, USA, and NASA Postdoctoral Program Fellow

⁵ Indian Institute of Astrophysics, 2nd Block 100 Feet Rd, Koramangala Bangalore, 560 034, India

⁶ Heidelberg University, Grabengasse 1, 691 17, Heidelberg, Germany

Accepted 2023 June 28. Received 2023 June 28; in original form 2023 April 27

ABSTRACT

The detection and accurate astrometry of fast-moving near-Earth objects (NEOs) has been a challenge for the follow-up community. Their fast apparent motion results in streaks in sidereal images, thus affecting the telescope’s limiting magnitude and astrometric accuracy. A widely adopted technique to mitigate trailing losses is non-sidereal tracking, which transfers the streaking to background reference stars. However, no existing publicly available astrometry software is configured to detect such elongated stars. We present *Astreaks*, a streaking source detection algorithm, to obtain accurate astrometry of NEOs in non-sidereal data. We validate the astrometric accuracy of *Astreaks* on 371 non-sidereally tracked images for 115 NEOs with two instrument set-ups of the GROWTH-India Telescope. The observed NEOs had V-band magnitude in the range [15, 22] with proper motion up to 140″/min, thus resulting in stellar streaks as high as 6.5′ (582 pixels) in our data. Our method obtained astrometric solutions for all images with 100% success rate. The standard deviation in Observed-minus-Computed (O-C) residuals is 0.52″, with O-C residuals <2″ (<1″) for 98.4% (84.4%) of our measurements. These are appreciable, given the pixel scale of ~0.3″ and ~0.7″ of our two instrument set-ups. This demonstrates that our modular and fully-automated algorithm helps improve the telescope system’s limiting magnitude without compromising astrometric accuracy by enabling non-sidereal tracking on the target. This will help the NEO follow-up community cope with the accelerated discovery rates and improved sensitivity of the next-generation NEO surveys. *Astreaks* has been made available to the community under an open-source license.

Key words: techniques: image processing – software: data analysis – astrometry – minor planets, asteroids: general – planets and satellites: detection

1 INTRODUCTION

Small Solar System bodies are remnants of the formation stage of the Solar System. These bodies encompass small natural objects like Near-Earth Objects (NEOs), main-belt asteroids, trans-Neptunian objects, and various other smaller groups of asteroids and comets. Their properties, such as size, shape, rotation and surface composition, are the result of collisions and dynamical evolution that has led to their formation. Asteroid science encompasses studies ranging from formation mechanisms, population, collisional evolution, orbital dynamics, compositional properties and physical mechanisms such as Yarkovsky and YORP effects (Michel et al. 2015). Out of all small solar system bodies, NEOs are of particular interest to the planetary science community, not only from a scientific perspective but also because of the hazardous consequences of their impacts on civilization (Perna et al. 2013). The planetary defence missions

to devise efficient mitigation strategies critically depend on timely detection and accurate knowledge of orbits and physical properties of these potentially hazardous asteroids (Reddy 2022; Nakano et al. 2022). The Double Asteroid Redirection Test (DART) mission is a planetary defence-driven test of technologies for preventing an asteroid’s impact on Earth, aimed at demonstrating the kinetic impactor technique for changing the motion of the moonlet of asteroid (65803) Didymos (Rivkin et al. 2021; Naidu et al. 2020; Thomas et al. 2023; Terik Daly et al. 2023). Several survey telescopes scan the night sky daily and report these NEO candidates to Minor Planet Center (MPC). With the current ground-based facilities, NEOs are typically discovered at a distance of less than 1 AU (Jedicke et al. 2016). At this distance, their apparent rate of motion can be high, thus challenging their follow-up and recovery.

Most of the telescope facilities operate in the sidereal mode during their regular operations. The high apparent motion of NEOs with respect to the far-situated background astrophysical objects results in a streak in the astronomical images. The quest of discovering and characterizing the NEOs is steered by robotic survey telescopes

* E-mail: kritti@caltech.edu

† E-mail: harshkumar@iitb.ac.in

with wide fields of view (Seaman et al. 2021a). These surveys detect NEOs by their apparent motion between successive exposures and submit the NEO candidates to the MPC. Usually, this discovery data consists of at least two detections, known as a “tracklet” (Kubica et al. 2007). The short observation arcs from the discovery data result in high uncertainties in the preliminary orbit estimate, which could lead to hundreds of arcseconds of uncertainties in the sky positions within a few hours after the discovery for the fastest, nearby, objects. Therefore, well-timed subsequent follow-up observations by meter-class telescopes like GROWTH-India Telescope (GIT; Kumar et al. 2022), with relatively wide fields of view are needed to affirm the candidacy of an NEO.

As discussed, due to sensitivity limitations of the current survey facilities, most of the candidates are discovered at a distance ≤ 1 AU on their discovery apparition (Jedicke et al. 2016). This results in a high apparent motion $\geq 10''/\text{min}$ that degrades the signal-to-noise ratio (SNR) of such candidates as the photons spread over a larger number of pixels in the form of a streak (Shao et al. 2014). Bright candidates create bright streaks that are detectable in such images, but fainter objects get blended into the background, causing a reduction in the detection limit of these objects compared to other sidereal targets. Furthermore, most of the NEO discovery engines like Zwicky Transient Facility (ZTF; Bellm et al. 2018), Catalina Sky Survey (CSS; Christensen et al. 2018), Asteroid Terrestrial-impact Last Alert System (ATLAS; Tonry et al. 2018) and Panoramic Survey Telescope and Rapid Response System (Pan-STARRS; Chambers et al. 2016) are located in North America and Hawaii island, which means that there are large geographical gaps between the discovery system and follow-up systems, typically in North and South America. Together, these factors make the recovery of NEOs in sidereally-tracked data quite challenging.

The 70-cm fully-robotic GIT was set up as a part of the international collaboration “Global Relay of Observatories Watching Transients Happen” (GROWTH; Kasliwal et al. 2019). GIT (MPC Observatory Code: N51), located at the Indian Astronomical Observatory, Hanle-India, has a 16.8-megapixel sensor which provides a large field of view of 0.5 deg^2 , thus making it an excellent tool of the trade for NEO follow-up campaigns. Furthermore, its geographical location at Hanle is on the opposite side of Earth to the major NEO discovery engines, allowing us to observe the candidates before the positional uncertainties blow up to unmanageable scales (Sharma et al. 2021).

The next generation NEO survey programs like NEO Surveillance Mission (NEOSM; Grav et al. 2020) and Vera C. Rubin Observatory’s Legacy Survey of Space and Time (LSST; Vera C. Rubin Observatory LSST Solar System Science Collaboration et al. 2021) are expected to increase the number of NEOs discoveries with absolute magnitude, $H < 22$ mag by 26% (corresponding discovery rate $\sim 2\times$) against the existing surveys over a period of 10 years of its planned operations (Jones et al. 2018), along with the need of deep limiting magnitude follow-up $r \sim 24.5$ mag (Chesley & Veres 2017). As typical depth probed by small telescopes in a reasonable sidereal exposure is around $V \sim 22$ mag, LSST and NEOSM together will increase the depth requirements of follow-up facilities by couple of magnitudes (Seaman et al. 2021b). This indicates an emerging need to improve the limiting magnitude of the follow-up telescope campaigns of such fast-moving NEOs. The NEO follow-up community can mitigate the damaging effects of trailing losses by tracking at the rate of NEO’s apparent motion instead of the stars with existing facilities, thus preserving the point spread function of the NEO (Vereš et al. 2012). This non-sidereal tracking improves the system’s limiting magnitude for fast-moving objects by transferring the trailing to background reference stars. However, the astrometric measurement

with the trailing stars is a challenging task with existing software that assume largely symmetric point spread functions. These software are not designed to obtain astrometry with elongated reference stars. Moreover, most of these software require human intervention to perform various tasks, which will be a bottleneck in the follow-up campaigns with the advent of the next-generation survey telescopes. Therefore, in order to complement the self-follow-up strategies of these surveys, we look forward to robust astrometry techniques to support the improvement in NEO orbital catalogues.

Here, we present a novel source detection algorithm, *Astreaks* — Astrometry with Streaking Stars, to obtain an astrometry solution for astronomical images with elongated reference stars¹. Developed for GIT, *Astreaks* achieves the goal of accurate astrometry using the image segmentation technique, implemented using publicly available astronomy python packages. The pipeline has been validated on two different instrument set-ups and achieves sub-arcsecond astrometric accuracy. The operations of our fully-automated pipeline can be easily transferred to any other telescope system due to its modular nature with minor modifications in the configuration file. This article is organized as follows. In § 2, we review the loss in astrometric accuracy and limiting magnitudes due to trailing losses, existing methods to recover these trailing losses, and the benefits of non-sidereal tracking. We elaborate on the analysis framework of our elongated source detection algorithm and validate the astrometric accuracy of *Astreaks* in § 3. Finally, we conclude with a summary and future outlook in § 4.

2 SIDEREAL & NON-SIDEREAL OBSERVATIONS

Sidereal observations are where we track the motion of the stars across the sky. To perform the observations in sidereal mode, the telescope motion is corrected for the motions of the stars around the north celestial pole. This helps us keep the star’s image focused on the same group of pixels even when the stars are moving around the pole. However, solar system objects usually have a different sky plane motion compared to the stars. Therefore, unlike stars, these objects do not result in the typical 2D Gaussian profile in an image. The minor planets are an example of such objects which leave trails in sidereally-tracked exposures due to their significant apparent rate of motion. The light from these objects spread over many pixels along their motion, causing streaks in the images (Figure 1). These streaks result in a decrease in the signal-to-noise ratio of the source, which leads to two effects – a decrease in the detection sensitivity and a decrease in astrometric accuracy for such objects.

As discussed above, the trailing of minor planets in the sidereal image spreads the flux from the object over a larger area. This causes a reduction in the target’s apparent magnitude per unit area and hence signal-to-noise ratio (Krugly 2004). To demonstrate these effects, we observed the NEO, 2000 NM in sidereal as well as non-sidereal mode, where we tracked the motion of the NEO rather than the stars in the background. We conducted these observations on 2022-08-04 at 16:31:57.0 UTC, where we took 5 minute-long sidereal and non-sidereal exposures. Figure 1 shows the trailing loss in sidereal exposure for the NEO when compared against its non-sidereal exposure. The target was moving at an apparent rate of $4.01''/\text{min}$, and the typical seeing during our observations was $2.65''$. Therefore, the target streaked in the sidereal exposure with an aspect ratio of

¹ This work was also presented at the European Planetary Science Congress 2021 (Sharma et al. 2021).

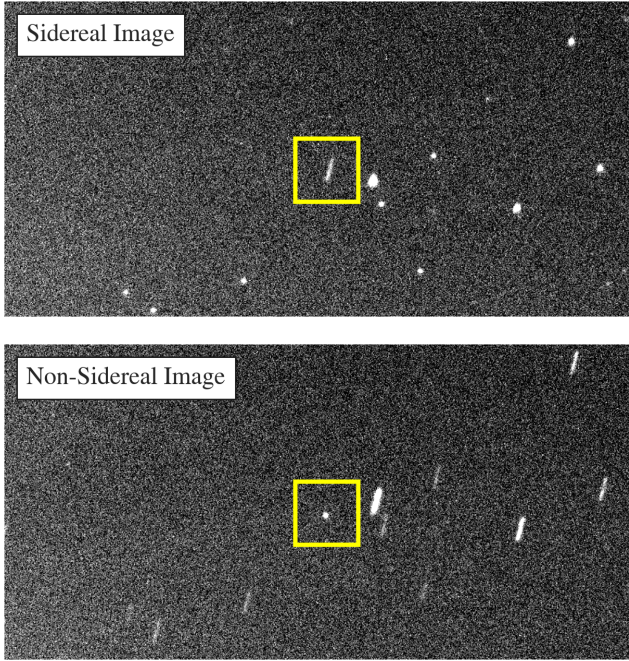


Figure 1. Comparison of sidereal (upper panel) and non-sidereal (lower panel) images for 2000 NM, a NEO with an apparent motion of $\sim 4''/\text{min}$ during our observations. The target streaks in the sidereal exposure and this streaking gets transferred to background reference stars in the non-sidereal exposure. The resulting loss in the signal-to-noise ratio of the target in sidereal exposure is $\sim 20\%$, primarily due to trailing losses.

$\ell/w \sim 3.8$. The signal-to-noise ratio of the target’s streak in sidereal exposure is 13.0. A similar measurement on the non-sidereal exposure for the target yields a signal-to-noise ratio of 16.4. Therefore, we observe a $\sim 20\%$ loss in the signal-to-noise ratio of the target in the sidereal exposure compared to non-sidereal exposure. This loss of signal-to-noise ratio of the trailed object reduces the limiting magnitude of the system for such fast-moving asteroids, thus reducing the probability of detection for these NEOs in sidereally-tracked astronomical images (Rabinowitz 1991).

Along with the decrease in the limiting magnitude of the system, these streaks in the sidereal observations also affect the astrometric measurements. Astrometric measurements in images with significant elongations require non-trivial techniques like “trail fitting” (Vereš et al. 2012). Furthermore, it has been tested that the astrometric accuracy of the trail-fitting algorithm is compromised at low SNR (Vereš et al. 2012). Thus, the reduced SNR of the target in sidereally-tracked astronomical images results in increased uncertainty in astrometric measurements of the streaked NEOs. This loss in astrometric accuracy due to trailing losses is even more important for fast-moving NEOs in the discovery apparition since their recovery is dependent on accurate astrometry.

Over the years, several image processing techniques have been proposed to recover the target and improve both astrometry and photometry of the target in sidereally-tracked data. The working principle of a majority of these is based on the “shift-and-add” technique to enhance sensitivity (Cochran et al. 1995; Tyson et al. 1992; Parker & Kavelaars 2010). In this technique, we acquire several sidereally-tracked short exposures of the field, which are then shifted based on the known velocity vector of the minor planet and co-added to improve its signal-to-noise ratio. We illustrate a basic implementation of this technique in Figure 2 on sidereally-tracked data for Comet

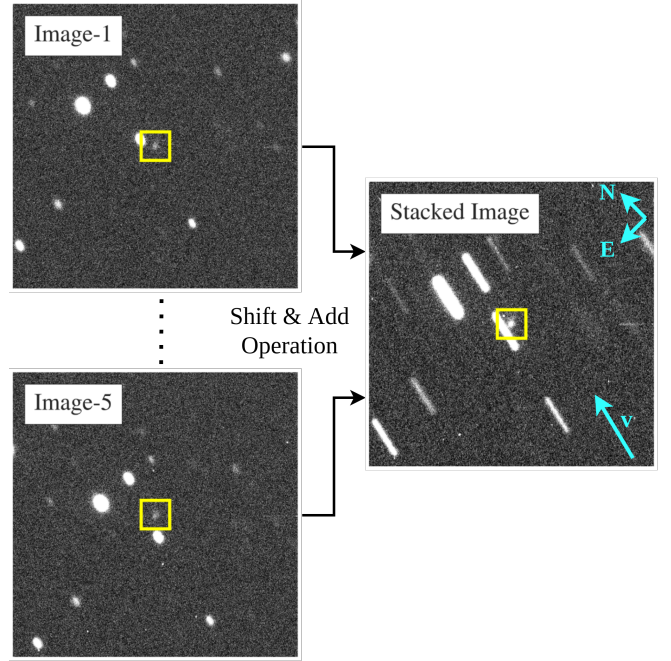


Figure 2. Illustration of shift and add operation when implemented on sidereally-tracked data of Comet C/2021 A4 (NEOWISE). The comet had a sky-plane motion of $1.33''/\text{min}$ and an apparent magnitude >20 at the time of our observations. We observe that on co-adding the frames with appropriate shifts for the motion of the comet, we get $\gtrsim 3$ -fold amplification in the signal-to-noise ratio of the comet in our data as compared to single images.

C/2021 A4 (NEOWISE; Mainzer et al. 2021). These observations were conducted at the discovery apparition of this comet and were consequently submitted to MPC. The comet had a proper motion of $1.33''/\text{min}$ at a position angle of 342.9° during our observations. The average signal-to-noise ratio in five individual sidereally-tracked images is ~ 25 , which got amplified to ~ 88 in the stacked image. This improved signal-to-noise ratio enables us to recover faint targets, overcome trailing loss, and confidently detect cometary activity. However, this technique is sub-optimal for fast-moving objects due to its requirement of astrometry solutions for individual images. Such objects require short exposure times to retain their Gaussian point spread function, thus resulting in less reference stars in the field to obtain astrometry solutions. Furthermore, short exposure time causes a significant loss in observing efficiency due to multiple readout cycles. Moreover, this technique requires the exposure to be long enough to detect the faint objects in individual images. This results in measurable elongation in the point spread function of the NEO, thus compromising the astrometric accuracy.

Vereš et al. (2012) used an analytical form of trailing function for trail fitting to yield accurate astrometry and photometry. However, this technique has limited usage for astrometry of faint, fast-moving NEOs observed with small telescopes. Moreover, the loss in photometric and astrometric accuracy increases with higher trail aspect ratios and lower signal-to-noise ratios. Gural et al. (2005) developed a matched-filter-based trail detection technique, which attempts to integrate multiple frames by shifting and stacking based on a hypothesis of the target’s velocity and then matched-filtering using the hypothesized template. Shucker & Stuart (2008) proposed a similar velocity matched-filter-based approach to integrate multiple frames, which increases the aggregate signal-to-noise ratio using a multi-hypothesis velocity vector. These methods are computationally ex-



Figure 4. Illustration of the sky background estimation technique used in *Astreaks* on non-sidereally tracked image for 2020 XB acquired on 2020-12-01 at 17:09:48 UTC (left panel). A gradient is present in the image because the moon was only 38° from the target

at the time of observations, which is appropriately captured by our sky background estimate (middle panel). Before proceeding, we subtract this sky background from our science image, as displayed in the right panel.

ground estimation technique. It then creates a synthetic image which is eventually used to obtain the astrometric solution. The following sections highlight the detailed working of the pipeline.

3.1 Sky Background Estimation

Accurate background estimation is crucial for detecting faint sources and determining the correct fluxes from each source. The presence of streaking background reference stars affects the background statistics, due to which, the traditional methods fail to get an accurate background map of the image. To estimate the background, we overlay a grid on the entire image and calculate the mode of counts in each of the cells in this grid: giving a nominal background level for each grid point. We note that mode is a better estimator than the median, as there can be a large number of extended sources which add a heavy tail to the histogram of counts in each grid cell. The grid spacing has to be chosen by keeping in mind the presence of extended sources and occasional crowded fields. If cells are too small, extended sources may dominate some cells and the background estimate will be compromised. If the cells are too large, we will be insensitive to background variations at smaller scales. We recommend that the mesh size should be at least greater than the streaks in the image to avoid detecting the streak itself in the background when using mode as an estimator. Future versions of *Astreaks* will incorporate an automated mesh size based on the tracking rate and exposure time that determines the length of the stellar streaks. Next, we create a smooth background estimate from these background measurements. In our data, we found that using a linear background variation over the entire image gives satisfactory results. Hence, we fit a plane to this background data by least-squares minimization and subtract this from the original (un-gridded) image. Typically the NEOs observed with GIT have a proper motion of the order of $10''/\text{min}$, and the typical exposure time is 3 minutes. An average pixel scale of $0.5''/\text{pix}$ amounts to streaks of length ~ 50 pixels. Testing 371 images of 115 NEOs, we observed that meshes of size 60 – 100 pixels work well.

Figure 4 shows our sky background estimation technique on the observations of the minor planet 2020 XB. A background gradient is present in the image because the moon was only 38° from the target. This background gradient is appropriately captured in our corresponding sky background estimate. We subtract this sky background from our image before further analysis.

3.2 Streak Spread Function Model Generation

Streaked sources in the image can be thought of as a convolution of the PSF of the telescope system and the motion vector of the source in the image (Long et al. 2020). Therefore, estimating this “streak spread function” (SSF) model is necessary to detect the streaking reference stars. We measure the full width at half maximum (FWHM) of the streaks perpendicular to the direction of motion of the target, and create a 2-D Gaussian PSF with the same FWHM. The angle of the streak with respect to image orientation is estimated using *opencv* package (Bradski 2000). We use *opencv*’s sigma threshold module to detect streaked objects in the image, and from that, we can get the orientation/angle of the streaks. Further, we compute the expected length of the streak using the tracking rate and exposure time of the image. In the process, we generate a horizontal aggregation of point sources spaced by 1 pixel and spanning across the length of the streak. For more smoother sampling of SSF, the aggregation of point sources spacing can be decreased to a sub-pixel level depending upon the available computational power. This line is then convolved with the Gaussian PSF model and rotated by the computed streak position angle to generate the final SSF model of the streaking stars (Vereš et al. 2012) using the *Astropy* (Astropy Collaboration et al. 2013, 2018) python package.

Figure 5 compares an original stellar streak in the data acquired for the minor planet 2020 UA1, observed during its discovery apparition, with the corresponding SSF model generated by *Astreaks*. The apparent rate of motion of the target was $39.25''/\text{min}$ at the time of our observations, thus leading to $78.5''$ long stellar streaks in the data in exposures of two minutes. The calculated position angle of the target using the velocity position angle (118.2°) and telescope position angle (-52.3°) is $\sim 66^\circ$, which is consistent with our orientation measurement with the sigma-thresholding algorithm. The SSF generated using these parameters accurately represents the stellar streak shown in the figure.

3.3 Source Detection

We use the background subtracted image to detect sources. For this purpose, we generate a 1σ threshold (a configurable hyper-parameter, see Table 1) for the image and apply that to detect the sources. Such a low threshold has been chosen to detect the faint sources in the image. After that, image segmentation is performed on the background-subtracted image with a normalised SSF model as the kernel using the *photutils* (Bradley et al. 2020) python packages. The kernel identifies the pixels with counts greater than the corresponding

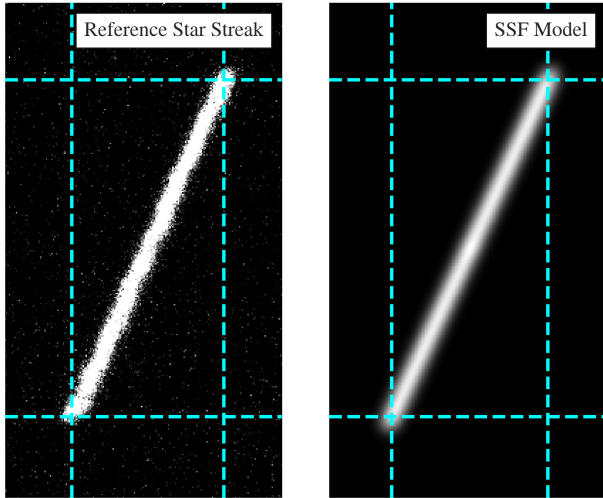


Figure 5. Comparison of a reference star streak in the 2020 UA1 non-sidereally tracked image (left panel) and the corresponding SSF generated by our pipeline (right panel). The computed start and end points of the streak are marked. The SSF model generated by convolving the PSF model from the non-sidereal image and ideal streak model, which is a line joining these endpoints, appropriately models the reference star streak.

pixel-wise threshold level. Next, the pipeline identifies the group of pixels corresponding to the same source using the streak length. The segmented sources are then deblended to separate the overlapping sources. The flux inside the elliptical apertures measures the flux from each source. The deblending routine further computes the deblended flux and corresponding flux errors for overlapping sources. The `photutils` python package provides a good measure of flux for deblended sources, hence we chose to use the flux of these sources using the elliptical aperture. We create a “detected source catalogue” comprised of the centroids, total flux and flux errors of each source.

The sources detected by the pipeline in a representative non-sidereally tracked image of 2020 UA1 are highlighted in the top panel of Figure 6. The target NEO is marked with a yellow rectangular box. The blue dots represent the positions of background stars at the mid-time of the exposure that is used as reference stars in a later stage. A few of the streaks lie close to the edge; hence, their centroid location and flux estimation is incorrect as shown by orange marks in the top panel of Figure 6. To remove any biases due to these sources, we remove the streaks whose centroid falls within half the streak length from the edges, denoted by red dashed lines.

3.4 Obtaining an Astrometric Solution

Next, we use our detected source catalog to generate a synthetic image. A specific advantage of this method is that the synthetic image is broadly similar to the images that would be acquired by the telescope with sidereal tracking. Hence, the usual astrometry pipelines used for that telescope can be used directly for processing this synthetic image. We use a 2-D gaussian PSF, with the same sigma as the “SSF” in §3.2 as our model for point sources in the image. Starting with a blank image, we use this PSF model to inject a source with appropriate flux at the location of each detected source. We do not consider the sources near edges whose properties are known to be inaccurate. The median sky background and its root mean square value estimated from the original image is added to the synthetic image. The resulting synthetic image is shown in lower panel of

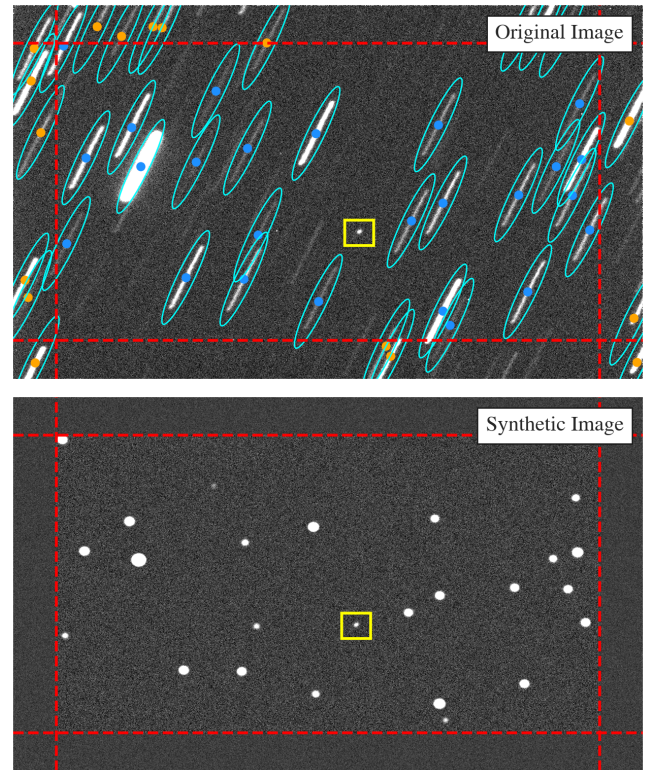


Figure 6. Detection of background reference stars using `Astreaks` in a non-sidereally tracked image of 2020 UA1. The detected sources at mid-time of the exposure are marked as dots on top of the corresponding source’s streak in the top panel. We replace the streaked sources with their flux-scaled gaussian equivalent sources in a synthetic image, as displayed in the bottom panel and obtain the WCS solution of the resultant synthetic image. During this process we neglect the sources lying close to the image edge (sources marked with orange color in top panel) and perform astrometry of the target at the mid-time of the exposure.

Figure 6. This synthetic image is then solved for the World Coordinate System (WCS) using the offline engine of `astrometry.net` (Lang et al. 2010). We use the WCS of this synthetic image as the astrometric solution for the original image at the mid-time of the exposure.

3.5 Astrometry, Photometry, and Orbit Determination

The astrometric positions of the target NEO at the mid-time of the exposure are obtained using the WCS of the synthetic image. Target asteroids are often faint even in non-sidereal tracked exposures. Automated searches for it often give false positives. Since the user is aware of the approximate location of the NEO, at this stage, the NEO is first visually identified. Then, its exact position is determined by fitting the 2-D Gaussian PSF from §3.4. We compute the instrumental magnitude of the target using aperture photometry (Bradley et al. 2020), using the source fluxes measured in the source detection step (§3.3). The magnitudes of streaked stars are cross-matched with the Pan-STARRS catalogue (Flewelling 2018) using `VizieR` query to calculate the zero points. This zero point is directly used to calculate the magnitude of the point source NEO in the image. Our photometry is accurate to ~ 0.2 mag and further improvement in the photometric accuracy in progress. We append our astrometric and photometric measurements to the existing observations of the target at MPC and attempt an orbit fit using `find_orb` (Gray 2011) to

compute the Observed-minus-Computed (O-C) residuals. These O-C residuals are a direct measurement of the astrometric uncertainty.

3.6 Hyperparameters and Parameters

Astreaks requires various inputs for its modular functioning, which are summarized in Table 1. The astrometry configuration of the pipeline comprises several *hyperparameters* that depend on the instrument properties and are the same for all targets being analysed. Hyperparameters like mesh size, pixel scale, threshold level, the maximum size of the PSF model etc., are required at different stages of source extraction and measurements. An appropriate mesh size depends on the typical length of the streaks in data and plays a primary role in estimating a reliable sky background. The SSF model generation requires pixel scale information to compute streak parameters. Based on the instrument's sensitivity, the threshold and contrast levels are required for source detection. The synthetic image generation requires the maximum PSF model's size which is fixed based on the typical full width at half maximum (FWHM) of the PSF for the telescope system. The photometry of the target requires the camera properties like the gain of CCD, which is typically fixed for a single instrument. All these hyperparameters must be set up for the best results before using the pipeline on a new instrument.

Apart from the hyperparameters discussed above, Astreaks requires a set of *parameters* that must be updated for each target. These include tracking rate, velocity position angle and exposure time which are different based on the target of interest. A combination of these parameters determines the streak parameters and size. The pipeline extracts these parameters automatically using the information stored in the image headers and performs the astrometric operations on the image. Further, the pipeline can generate an automated MPC report once we specify the pixel coordinates of the target.

3.7 Astreaks Validation

Astreaks has been developed on data acquired with GIT. For this purpose, we used observations of 115 NEOs covering a wide range of proper motion. To test the robustness of Astreaks, we acquired data on two CCD camera set-ups: Apogee KAF3200EB (Apogee hereafter) and Andor iKon-XL 230 4k back-illuminated CCD (Andor hereafter). As both cameras have different properties, they provide a nice framework to test the reliability and modularity of Astreaks. Apogee camera has a narrow $\sim 11' \times 7.5'$ field of view (FOV) camera with a pixel scale of $0.307''/\text{pix}$. On the other hand, Andor has a $\sim 45.87' \times 45.74'$ FOV with $0.67''$ pixel scale.

The data used for Astreaks development and validation was acquired from September 2020 to December 2022. 64% of these data are wide field images acquired with Andor camera, the rest were obtained with the narrow FOV Apogee Camera. A total of 18 NEOs were observed with the Apogee camera, amassing 133 non-sidereal images during the initial phase of Astreaks development. These targets had a proper motion in the range of $4 - 120''/\text{min}$ at the time of observation, resulting in $14 - 140''$ long streaks of reference stars in exposures up to 5 minutes. Using Astreaks, we obtain astrometric measurements of these NEOs following the procedure outlined in §3. The O-C residuals in right ascension and declination were computed using the `find_orb` (Gray 2011) software by appending all observations of these targets at the MPC database. These O-C residuals

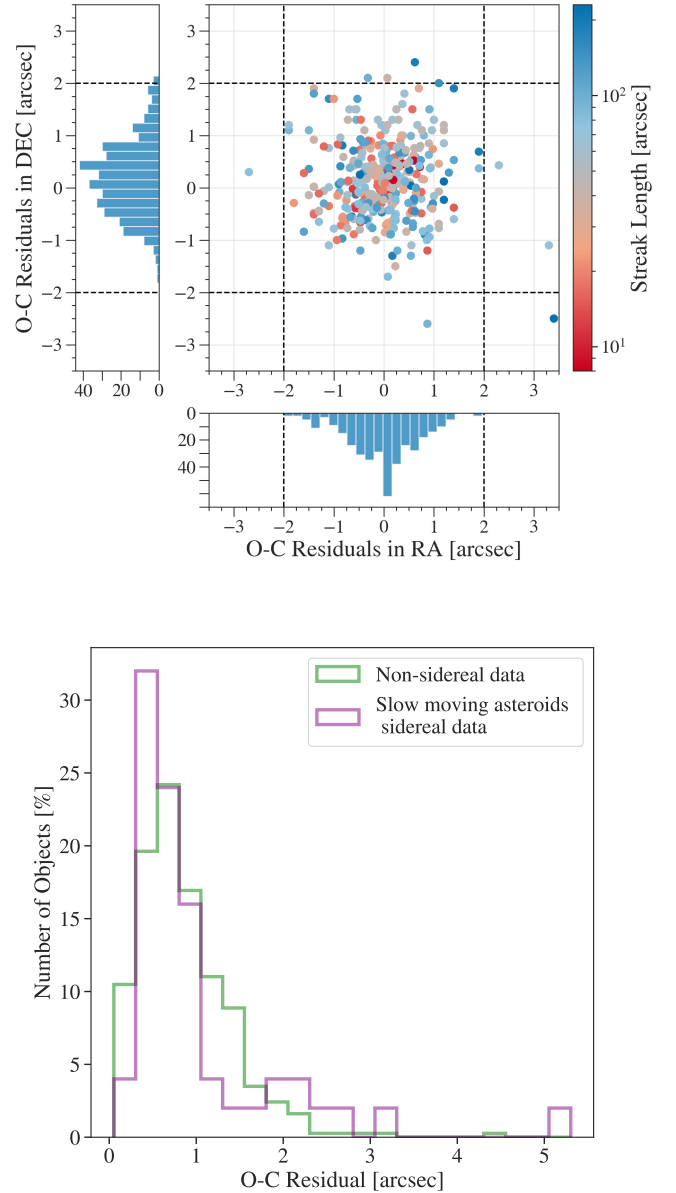


Figure 7. Validation of the astrometric accuracy of Astreaks. Upper panel: Validation using O-C residuals in right ascension (RA) and declination (DEC) for 371 positions of 115 NEOs observed with GIT using non-sidereal tracking. The standard deviation of all these measurements is $0.52''$. Lower panel: Comparison of O-C residuals from Astreaks reduction of non-sidereal data and slow-moving asteroids in sidereal images reduced using standard procedures. The performance of Astreaks on non-sidereal data is similar to that of normal astrometric measurements from sidereal images.

have a standard deviation of $0.41''$, which qualifies the $< 2''$ quality of measurements criterion, as demanded by MPC².

Once the working and scientific reliability were established with Apogee data, we used 238 non-sidereally tracked images for 96 NEOs acquired with Andor camera data to test the performance of the pipeline. By virtue of the modular nature of our pipeline, we could easily shift from the Apogee to Andor instruments by a simple tweak

² MPC's Guide to Minor Body Astrometry: <https://cgi.minorplanetcenter.net/iau/info/Astrometry.html>

Parameter Type	Name	Description
Hyperparameters	mesh size	The size of each block in the grid used for background estimation. Units: pixels
	pixel scale	The plate scale to convert the size of mesh in data to image pixels. Units: "/pixel
	thresholding level	The assumed background level to threshold the image and identify streaks.
	PSF model size	The maximum size of the PSF model to be used for generating the SSF. Units: pixels
	gain	The detector gain to scale instrumental counts to the number of electrons per pixel. Units: e ⁻ /ADU
Parameters	NEO tracking rate	The sky-plane velocity of the NEO to estimate the streak length. Units: "/min
	exposure time	The total non-sidereal exposure time to estimate the streak length. Units: sec
	velocity position angle	The velocity position angle of the NEO to determine the orientation of the SSF. Units: degrees
	image coordinates of the target	Pixel coordinates of the target in the image to fit a PSF and extract coordinates.

Table 1. The description of the set of parameters and hyperparameters used by *Astreaks*.

of hyperparameters, (see § 3.6). The NEOs had a proper motion in the range of 1–45"/min, resulting in 8–396" long stellar streaks in exposures of 1–9 minutes. The computed O-C residuals for astrometric measurements using *Astreaks* have a standard deviation of 0.58". The O-C residuals in RA and declination of all observed positions of 115 NEOs (371 images) are shown in the upper panel of Figure 7. More than 84.4% of our measurements have O-C residuals < 1", with 98.4% measurements exhibiting a < 2" astrometric accuracy. We found that the astrometric O-C residuals do not correlate with the streak length (Pearson r value: 0.0074).

We acknowledge that *Astrometrica* software is not designed to detect sources and obtain astrometry solutions with significant elongation in reference stars (Raab 2012). However, since no streak-analysis packages are publicly available, we compare our source detection capability and astrometric accuracy with *Astrometrica*. We illustrate this comparison on a representative example of non-sidereal data for 2020 UA1. We obtained a total of 9 exposures for 2020 UA1 among which only three images were astrometrically solved with manual cross-match using *Astrometrica*. On the other hand, *Astreaks* successfully solved all nine images with the algorithm discussed in §3. Furthermore, the number of sources detected by the *Astrometrica* software is less than that of *Astreaks*. Despite a manual cross-match, many bright sources are missed by *Astrometrica*, potentially responsible for the failure of the astrometric solution on the other six images. The number of sources plays a direct role in the quality of the astrometry solution and is higher for *Astreaks* due to the detection of a large number of sources as compared to *Astrometrica*. The standard deviation of astrometric measurements on nine images using *Astreaks* (0.2") is better than the astrometric accuracy on three images using *Astrometrica* (0.3"), thus validating that our algorithm is more accurate and robust for obtaining astrometric solutions of non-sidereal images.

As a final test, we also compare the astrometric capabilities of *Astreaks* with standard astrometry procedures on sidereal data. The total astrometric uncertainty for NEOs may include a component from the orbital uncertainty. Hence, for a fair comparison, we use a sample of 50 sidereal data of six slow-moving asteroids with apparent motion less than 0.58 arcsec/min during the exposures. These targets appeared as a point source in our astronomical images of exposure times less than 3 min, given the typical FWHM of PSF in sidereal data of ~3". Astrometry on these images was performed using our usual, standard astrometry procedures for sidereal data, as described in Kumar et al. (2022). A comparison of O-C residuals in sidereal data reduced following standard astrometry procedures and non-sidereal data reduced using *Astreaks* is shown in the lower panel of figure 7. We observe that the performance of *Astreaks* on non-sidereal data is comparable to normal astrometry methods on sidereal data.

4 CONCLUSION AND FUTURE PROSPECTS FOR ASTREAKS

This work presents the first open-source astronomy package to do accurate astrometry of non-sidereal tracked NEO images with significant elongation in reference stars — *Astreaks*. We use a novel method to perform astrometry on the non-sidereal tracked images. The pipeline uses a background estimation technique that appropriately captures the background variations while also considering the presence of elongated sources in the field. Further, we methodically compute the SSF of elongated sources by leveraging the knowledge of the telescope system PSF and observation parameters of the target. The pipeline has been designed to meet the goal of accurate astrometry with the novel technique of image segmentation and source de-blending on the background-subtracted image. The catalog of sources detected in this image is used to generate a synthetic image that imitates a sidereal image, had it been taken at the mid-time of the exposure. The astrometry solution of this synthetic image gives the astrometric measurements of the minor planet.

We validate the performance and results of the astrometric accuracy of *Astreaks* on non-sidereal data with GIT using two different instrument set-ups. We achieved an astrometric accuracy of 0.52" for 115 NEOs from 371 images, which had stellar streaks up to 6.5". This is well below the 2" threshold considered acceptable by the Minor Planet Centre. The astrometric results have been tested against the widely used software, *Astrometrica*, where we observe that *Astreaks* outperforms it in detecting elongated reference stars as well as in the accuracy of the astrometric solution for non-sidereal tracked images. A comparison of astrometry accuracy revealed that the performance of *Astreaks* on non-sidereal data is as good as point source astrometry in sidereal data. The modular nature and validation of the pipeline on two different set-ups emphasize that the pipeline can be integrated with other set-ups with simple tweaks in hyperparameters.

Astreaks is being used regularly on GIT for the analysis of asteroid data. Some results have been presented in Sharma et al. (2021). In the future, we aim to further improve the astrometric accuracy of *Astreaks* by accounting for the acceleration of NEOs when estimating the streak length for SSF model generation. Typically, the apparent rate of motion of NEOs is between $10^{-1} - 10^2$ arcsec/s with accelerations varying between $10^{-7} - 10^{-2}$ arcsec/s² (Vereš et al. 2012). For a NEO moving with an apparent angular velocity of 10^2 arcsec/s and an acceleration of 10^{-2} arcsec/s², the change in streak length during a 100 s exposure will be by 1". This is a significant change to impact our astrometric accuracy for such long-streaked objects, thus pointing towards the scope of further improvement in the astrometric measurement by *Astreaks*. In addition to astrometry, there is significant scope of improvement in photometric accuracy of *Astreaks* (work in progress). Secondly, we wish to

eliminate even the small manual step of identifying the approximate NEO location in the image, which is needed for centroiding and PSF fitting for astrometry and photometry. Lastly, the image segmentation process involves a convolution operation, which is an $O(N^2)$ operation for an $N \times N$ image, due to which the current implementation of Astreaks is time-consuming (\sim minutes on a generic desktop). Therefore, for faster data processing and submission of observations, we will attempt to make the aforementioned step more time efficient in subsequent versions of the pipeline.

ACKNOWLEDGMENTS

The GROWTH India Telescope (GIT) is a 70-cm telescope with a 0.7-degree field of view, set up by the Indian Institute of Astrophysics and the Indian Institute of Technology Bombay with support from the Indo-US Science and Technology Forum (IUSSTF) and the Science and Engineering Research Board (SERB) of the Department of Science and Technology (DST), Government of India. It is located at the Indian Astronomical Observatory (Hanle), operated by the Indian Institute of Astrophysics (IIA). We acknowledge funding by the IITB alumni batch of 1994, which partially supports operations of the telescope. Telescope technical details are available at <https://sites.google.com/view/growthindia/>.

Kritti Sharma thanks Michael S. P. Kelley (U. Maryland) for his valuable guidance in comet photometry. Kritti Sharma thanks Kunal Deshmukh (IITB) for his guidance during sidereal observations. Harsh Kumar thanks the LSSTC Data Science Fellowship Program, which is funded by LSSTC, NSF Cybertraining Grant #1829740, Brinson Foundation, and Moore Foundation; his participation in the program has benefited this work. B.T.B. is supported by an appointment to the NASA Postdoctoral Program at the NASA Goddard Space Flight Center, administered by Oak Ridge Associated Universities under contract with NASA. This research has made use of data and/or services provided by the International Astronomical Union's Minor Planet Center (<https://www.minorplanetcenter.net/iau/mpc.html>). This work has made use of the `find_orb` (Gray 2011) software supplied by Project Pluto (https://www.projectpluto.com/find_orb.html). This research has made use of Astrometrica (Raab 2012) software (<http://www.astrometrica.at/>). This research has made use of the VizieR catalogue access tool, CDS, Strasbourg, France. (DOI:10.26093/cds/vizie). The original description of the VizieR service was published in 2000, A&AS 143, 23. This research has made use of Astropy (Astropy Collaboration et al. 2013, 2018), NumPy (Harris et al. 2020), SciPy (Virtanen et al. 2020), Matplotlib (Hunter 2007), Astro-SCRAPPY (McCully & Tewes 2019), SExtractor (Bertin 2011a), PSFEx (Bertin 2011b) and `astrometry.net` (Lang et al. 2010) software. This research has made use of NASA's Astrophysics Data System.

DATA AVAILABILITY

Astreaks has been made available to the community under an open source license.

REFERENCES

- Astropy Collaboration et al., 2013, *A&A*, **558**, A33
 Astropy Collaboration et al., 2018, *AJ*, **156**, 123

- Bellm E. C., et al., 2018, *Publications of the Astronomical Society of the Pacific*, **131**, 018002
 Bertin E., 2011a, in Evans I. N., Accomazzi A., Mink D. J., Rots A. H., eds, *Astronomical Society of the Pacific Conference Series Vol. 442*, *Astronomical Data Analysis Software and Systems XX*. p. 435
 Bertin E., 2011b, in Evans I. N., Accomazzi A., Mink D. J., Rots A. H., eds, *Astronomical Society of the Pacific Conference Series Vol. 442*, *Astronomical Data Analysis Software and Systems XX*. p. 435
 Bradley L., et al., 2020, *astropy/photutils*: 1.0.1, doi:10.5281/zenodo.4049061, <https://doi.org/10.5281/zenodo.4049061>
 Bradski G., 2000, *Dr. Dobb's Journal of Software Tools*
 Chambers K. C., et al., 2016, arXiv e-prints, p. arXiv:1612.05560
 Chesley S. R., Veres P., 2017, arXiv e-prints, p. arXiv:1705.06209
 Christensen E., et al., 2018, in *AAS/Division for Planetary Sciences Meeting Abstracts #50*. p. 310.10
 Cochran A. L., Levison H. F., Stern S. A., Duncan M. J., 1995, *ApJ*, **455**, 342
 Flewelling H., 2018, in *American Astronomical Society Meeting Abstracts #231*. p. 436.01
 Grav T., et al., 2020, in *AAS/Division for Planetary Sciences Meeting Abstracts*. p. 208.03
 Gray B., 2011, *Find_Orb : Orbit determination from observations*
 Gural P. S., Larsen J. A., Gleason A. E., 2005, *AJ*, **130**, 1951
 Harris C. R., et al., 2020, *Nature*, **585**, 357
 Hunter J. D., 2007, *Computing in Science and Engineering*, **9**, 90
 Jedicke R., Bolin B., Granvik M., Beshore E., 2016, *Icarus*, **266**, 173
 Jones R. L., et al., 2018, *Icarus*, **303**, 181
 Kamiński K., Wnuk E., Gołębiewska J., Krużyński M., Kankiewicz P., Kamińska M. K., 2017.
 Kasliwal M. M., et al., 2019, *PASP*, **131**, 038003
 Krantz H., Pearce E. C., Avner L., Durney O., Sauve C., 2018, in Evans C. J., Simard L., Takami H., eds, *Society of Photo-Optical Instrumentation Engineers (SPIE) Conference Series Vol. 10702*, *Ground-based and Airborne Instrumentation for Astronomy VII*. p. 107024R, doi:10.1117/12.2312142
 Krugly Y. N., 2004, *Solar System Research*, **38**, 241
 Kubica J., et al., 2007, *Icarus*, **189**, 151
 Kumar H., et al., 2022, *AJ*, **164**, 90
 Lang D., Hogg D. W., Mierle K., Blanton M., Roweis S., 2010, *The Astronomical Journal*, **139**, 1782
 Long M., Soubro Y., Weiping N., Feng X., Jun Y., 2020, *ApJ*, **888**, 20
 Mainzer A. K., et al., 2021, *Minor Planet Electronic Circulars*, pp MPEC 2021-A207 : COMET C/2021 A4 (NEOWISE)
 McCully C., Tewes M., 2019, *Astro-SCRAPPY: Speedy Cosmic Ray Annihilation Package in Python*, *Astrophysics Source Code Library* (ascl:1907.032)
 Michel P., DeMeo F. E., Bottke W. F., 2015, *Asteroids IV*, doi:10.2458/azu_uapress.9780816532131.
 Naidu S. P., et al., 2020, *Icarus*, **348**, 113777
 Nakano R., et al., 2022, *Planetary Science Journal*, **3**, 148
 Parker A. H., Kavelaars J. J., 2010, *PASP*, **122**, 549
 Perna D., Barucci M. A., Fulchignoni M., 2013, *A&ARv*, **21**, 65
 Raab H., 2012, *Astrometrica: Astrometric data reduction of CCD images* (ascl:1203.012)
 Rabinowitz D. L., 1991, *AJ*, **101**, 1518
 Ramasawmy J., et al., 2022, arXiv e-prints, p. arXiv:2207.03914
 Reddy V., 2022, in *LPI Contributions*. p. 2035
 Rivkin A. S., et al., 2021, *Planetary Science Journal*, **2**, 173
 Seaman R., et al., 2021a, in *Bulletin of the American Astronomical Society*. p. 241, doi:10.3847/25c2cfef.9eb9da4e
 Seaman R., et al., 2021b, *Bulletin of the AAS*, **53**
 Shao M., Nemati B., Zhai C., Turyshev S. G., Sandhu J., Hallinan G., Harding L. K., 2014, *ApJ*, **782**, 1
 Sharma K., Kumar H., Bolin B., Bhalariao V., Anupama G., Barway S., 2021, in *European Planetary Science Congress*. pp EPSC2021-378, doi:10.5194/epsc2021-378
 Shucker B. D., Stuart J. S., 2008, in *Asteroids, Comets, Meteors 2008*. p. 8388
 Terik Daly R., et al., 2023, arXiv e-prints, p. arXiv:2303.02248

- Thomas C. A., et al., 2023, [arXiv e-prints](#), p. [arXiv:2303.02077](#)
- Tonry J. L., et al., 2018, [PASP](#), **130**, 064505
- Tyson J. A., Guhathakurta P., Bernstein G. M., Hut P., 1992, in American Astronomical Society Meeting Abstracts. p. 06.10
- Vera C. Rubin Observatory LSST Solar System Science Collaboration et al., 2021, in Bulletin of the American Astronomical Society. p. 236, [doi:10.3847/25c2feb.d8909f28](#)
- Vereš P., Jedicke R., Denneau L., Wainscoat R., Holman M. J., Lin H.-W., 2012, [PASP](#), **124**, 1197
- Virtanen P., et al., 2020, [Nature Methods](#), **17**, 261
- Weiner B. J., et al., 2018, in Observatory Operations: Strategies, Processes, and Systems VII. p. 107042H ([arXiv:1809.01180](#)), [doi:10.1117/12.2314265](#)
- Zhang Y., Wang J., Su J., Cheng X., Zhang Z., 2021, [AJ](#), **162**, 250